Pre-patterned ZnO nanoribbons on soft substrates for stretchable energy harvesting applications

Teng Ma,[1] Yong Wang,[1,2] Rui Tang,[3] Hongyu Yu,[3] and Hanqing Jiang[1,a)]
[1]*School for Engineering of Matter, Transport and Energy, Arizona State University, Tempe, Arizona 85287, USA*
[2]*Department of Engineering Mechanics, Zhejiang University, Hangzhou, Zhejiang 310027, China*
[3]*School of Electrical, Computer and Energy Engineering, Arizona State University, Tempe, Arizona 85287, USA*

(Received 18 March 2013; accepted 6 May 2013; published online 23 May 2013)

Three pre-patterned ZnO nanoribbons in different configurations were studied in this paper, including (a) straight ZnO nanoribbons uniformly bonded on soft substrates that form sinusoidal buckles, (b) straight ZnO nanoribbons selectively bonded on soft substrates that form pop-up buckles, and (c) serpentine ZnO nanoribbons bonded on soft substrates via anchors. The nonlinear dynamics and random analysis were conducted to obtain the fundamental frequencies and to evaluate their performance in energy harvesting applications. We found that pop-up buckles and overhanging serpentine structures are suitable for audio frequency energy harvesting applications. Remarkably, almost unchanged fundamental natural frequency upon strain is achieved by properly patterning ZnO nanoribbons, which initiates a new and exciting direction of stretchable energy harvesting using nano-scale materials in audio frequency range. © *2013 AIP Publishing LLC*. [http://dx.doi.org/10.1063/1.4807320]

I. INTRODUCTION

Piezoelectric materials, such as lead zirconate titanate (PZT),[1–4] barium titanate ($BaTiO_3$),[5,6] aluminum nitride (AlN),[7] and zinc oxide (ZnO)[8–11] have been utilized to convert mechanical vibration energy into electrical energy for portable or self-powered electronics, among many other applications, such as solar cells.[12,13] Specifically, "piezoelectric nanogenerator,"[8] first introduced in 2006, has boomed the applications of nano-scale piezoelectric materials for energy harvesting. One representative configuration of these piezoelectric nanogenerators is a nano-scale piezoelectric cantilever and the energy of mechanical vibration to be harvested is in the vicinity of the system fundamental frequency, which is usually in the high frequency domain for nano-scale materials.[14] In order to accommodate the development of consumer electronics, piezoelectric nanogenerators are expected to be able to integrate with wearable or stretchable devices and different approaches with success to some extent, such as limited stretchability, have been attempted.[2,3,5,7,8] The deformability, i.e., bendability and stretchability, is realized by bonding buckled piezoelectric materials on top of soft materials. There are two limitations among existing work, namely, energy harvesting only at the high frequency domain and stretchability. To address the limitation of energy harvesting near the fundamental frequency, nonlinear energy harvesting has been explored to achieve large response bandwidth by various approaches.[15–20]

Here, we report an approach to utilize pre-patterned ZnO nanoribbons on soft substrates to achieve buckled forms for stretchable energy harvesting applications within audio frequency range. Three pre-patterned ZnO nanoribbons in different configurations were studied in this paper, including (a) straight ZnO nanoribbons uniformly bonded on soft substrates that form sinusoidal buckles, (b) straight ZnO nanoribbons selectively bonded on soft substrates that form pop-up buckles,[21] and (c) serpentine ZnO nanoribbons bonded on soft substrates via anchors. These pre-patterned ZnO nanoribbons were first fabricated on silicon-on-insulator (SOI) wafers using dry etching and then brought and bonded with soft materials through transfer printing. The nonlinear dynamics and random analysis were conducted to obtain the fundamental natural frequencies and to evaluate their performance in energy harvesting applications. Remarkably, almost unchanged fundamental natural frequency upon strain is achieved by properly patterning ZnO nanoribbons, which initiates a new and exciting direction of stretchable energy harvesting using nano-scale materials in audio frequency range.

II. EXPERIMENTAL DETAILS AND METHODS

A. Experimental details

The fabrication of pre-patterned ZnO nanoribbons started from a 370 nm thick ZnO film sputtered on silicon-on-insulator (SOI) wafer, followed by annealing at 900 °C for better piezoelectric properties. Standard photolithography was then used to pattern ZnO nanoribbons, such as straight or serpentine nanoribbons (Fig. 1(a)). In order to transfer pre-patterned ZnO nanoribbons from SOI wafers to soft substrates, the top silicon layer (2 μm in thickness) served as a sacrificial layer to release pre-patterned ZnO nanoribbons from SOI wafer. This approach is able to fabricate high-quality two-dimensional ZnO nanostructures (defined by the photolithography) as the involved processes are on hard substrates. The free ZnO nanoribbons were then picked up by a

a)Email: hanqing.jiang@asu.edu

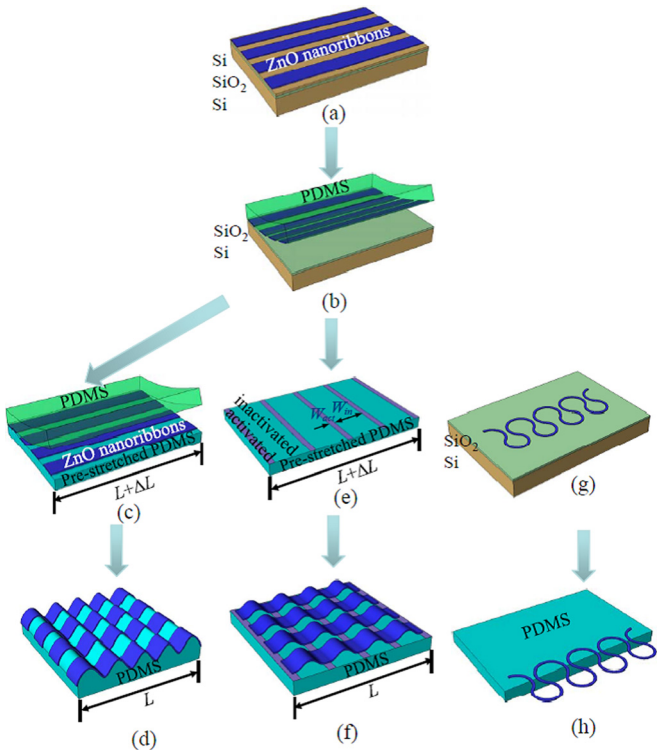

FIG. 1. Fabrication steps of pre-patterned ZnO nanoribbons on PDMS substrate. (a) Pre-patterned ZnO nanoribbons on a SOI wafer. Various patterns can be fabricated and here straight ZnO nanoribbons are illustrated. (b) After undercut-etching the sacrificial silicon layer, ZnO nanoribbons are picked up by a PDMS stamp. (c) ZnO nanoribbons are transferred to a pre-strained and uniformly treated PDMS substrate. (d) Relaxation of the pre-strain on PDMS leads to buckled ZnO nanoribbons on PDMS, which is referred as small waves. (e) Pre-strained PDMS substrates are treated by UV through an UVO mask to form periodically activated and inactivated areas. (f) ZnO nanoribbons are transferred to the pre-strained and selectively treated PDMS substrate, followed by relaxation of the pre-strain on PDMS, which leads to the pop-up buckling through the controlled delamination over the inactivated areas. This configuration is referred as big waves. (g) Serpentine ZnO nanoribbons rest on SOI wafer after the top silicon layer is etched away. (h) Serpentine ZnO nanoribbons are transferred to a PDMS substrate with one side hanging over. This configuration is referred as hanging-over serpentine.

polydimethylsiloxane (PDMS) stamp for transfer printing (Fig. 1(b)). The transfer printing is a process to transfer ZnO nanoribbons from a host substrate to a receiver PDMS substrate by using a PDMS stamp.

To enhance the interfacial bonding between ZnO and the receiver PDMS, the surface of receiver PDMS was treated by ultraviolet (UV) to form hydrophilic surface (terminated with $-O_nSi(OH)_{4-n}$ functionalities),[22,23] which is able to form strong chemical bonding through condensation reactions with various inorganic surfaces that have $-$OH groups (such as the surface of ZnO in the ambient environment). For the first configuration, the PDMS substrate was stretched by a pre-strain ε_{pre} ($= \Delta L/L$ for length changed from L to $L + \Delta L$) and then exposed to UV light for surface treatment. The ZnO nanoribbons on the PDMS stamp were laminated and aligned against the pre-strained and chemically treated receiver PDMS substrate along the direction of the pre-strain (Fig. 1(c)). As the bonding strength between the receiver PDMS and ZnO is stronger than that between the PDMS stamp and ZnO, peeling off the nanoribbons from the PDMS stamp led to transferring the ZnO nanoribbons onto the receiver PDMS. Releasing the pre-strain in the receiver PDMS substrate resulted in the spontaneous formation of sinusoidal buckled patterns (referred as small waves thereafter) due to mechanical competition between the stiff ZnO nanoribbons and soft PDMS substrate (Fig. 1(d)). For the second configuration of pre-patterned ZnO nanoribbons, the pre-stretched PDMS substrate was exposed to UV light through a ultraviolet-oxygen (UVO) mask[24,25] to generate selectively treated PDMS surface, namely activated area in width W_{act} for strong bonding and inactivated area in width W_{in} for weak bonding (Fig. 1(e)). Using the similar transfer printing approach, ZnO nanoribbons were transferred to a pre-stretched and selectively patterned receiver PDMS substrate. The relaxation of the pre-strain on the receiver PDMS caused ZnO nanoribbons on inactivated areas to delaminate from PDMS and form the periodic pop-up buckles anchored on activated areas (Fig. 1(f)). The patterns of pop-up buckles (referred as big waves thereafter) can be precisely controlled by the UVO mask. For the last configuration, the serpentine ZnO nanoribbons resting on the SOI wafer (Fig. 1(g)) were transferred to a receiver PDMS substrate anchored at one side to form a hanging-over serpentine structure (Fig. 1(h)).

B. Fabrication of ZnO nanoribbons on SOI wafer

A 370 nm thick ZnO film was deposited on a SOI wafer by RF sputtering with argon-oxygen (50/50) flow at power of 400 W and was then annealed at 900 °C to enhance the piezoelectric property. After that the ZnO film was patterned to ribbons by means of standard photolithography using AZ 4330 photoresist and subsequently wet-etched in ammonium chloride (NH_4Cl) solution. The underlayer silicon was etched using a xenon difluoride (XeF_2) vapor etching technique. The wafer was then placed in XeF_2 etching system (Model: Xetch E1, Xactic Inc.) for isotropic etching to remove the sacrificial silicon layer (etching pressure: 3000 mTorr, etching duration time per cycle: 60 s). Photoresist was stripped in acetone after silicon undercutting etching. ZnO ribbons were freed from their host substrate resting on SiO_2 layer without chemical bonding between them and were ready for transfer.

C. Fabrication of the UVO mask

Quartz slides coated with titanium (Ti), gold (Au), and photoresist were used as UVO masks. Before metal deposition, quartz slides were dipped into freshly prepared piranha solution (3:1 H_2SO_4/30%H_2O_2) for 1 h to remove organic impurities. After rinsing in deionized water and drying with a N_2 gun, cleaned slides were coated with 5 nm Ti and then 100 nm Au by E-beam evaporator at ultra-high vacuum (UHV). Ti was used as adhesion layer for Au and Au was employed as the mask layer for UV light. Negative photoresist SU-8 2015 (MicroChem) was spin-coated on the slides for 30 s at 4000 rpm to obtain a 13 μm-thick thin film. Standard lithography process was then performed to pattern SU-8 2015 and residue photoresist was then removed in an oxygen plasma asher leaving the desired photoresist pattern as hard mask for final Ti/Au etching. The exposed Au and Ti

areas were etched in gold etchant (TFA) for 1 min and titanium etchant (1:1:20 $HF/H_2O_2/H_2O$) for 30 s, sequentially.

D. Preparation of PDMS substrates

PDMS was prepared by mixing silicone elastomer base and curing agent (Sylgard 184, Dow Corning) at the ratio of 10:1 by weight, pouring into a petri dish, and baking at 80 °C for 3 h. Rectangular slabs of 1.5 cm by 6 cm were cut from the polymerized piece. Rinse the slab with isopropyl alcohol (IPA) to remove contaminations and dry it using a N_2 gun. A custom made stage was utilized to stretch the PDMS to specific strain levels. The pre-strained PDMS substrate was subjected to a flood exposure by a UV light (low pressure mercury lamp, BHK), which produces 185 nm and 254 nm radiations, for 150 s. The 185 nm radiations produce ozone, while the 254 nm radiations dissociate the ozone to O_2 and atomic oxygen (O) to form a chemically activated surface.

III. RESULTS

Figure 2(a) shows a tilted-view scanning electron microscopy (SEM) image of the small wavy ZnO nanoribbons on PDMS with 5% pre-strain. The wavelength was measured as $\lambda = 60.2\,\mu$m, which can be captured by the theoretical analysis[26] that gives buckling wavelength as $\lambda = 2\pi h_{\mathrm{ZnO}}[E_{\mathrm{ZnO}}(1-\nu_{PDMS}^2)/3E_{PDMS}(1-\nu_{\mathrm{ZnO}}^2)]^{1/3}$, where h is the thickness, E is the Young's modulus, ν is the Poisson's ratio, and the subscripts refer to ZnO nanoribbons and PDMS substrate. When the following literature values for the mechanical properties ($E_{\mathrm{ZnO}} = 129$ GPa, $\nu_{\mathrm{ZnO}} = 0.349$, $E_{PDMS} = 2$ MPa, and $\nu_{PDMS} = 0.48$) are used,[27,28] the theoretical solution gives $\lambda = 61.8\,\mu$m, which agrees very well with experiments without any parameter fitting. Figure 2(b) shows a tilted-view SEM image of big waves with $W_{act} = 20\,\mu$m, $W_{in} = 480\,\mu$m, and $\varepsilon_{pre} = 60\%$. The buckling wavelength was measured as 292 μm, which also agrees well with the theoretical analysis[29] $\lambda = W_{in}/(1+\varepsilon_{pre}) = 300\,\mu$m. Figure 2(c) shows the hanging-over serpentine ZnO nanoribbons. The width of serpentine ribbon is 100 μm. These three configurations of patterned ZnO nanoribbons all present excellent stretchability. The small waves and big waves (Figs. 2(a) and 2(b)) are stretchable through the change of buckling profiles. For example, upon tension, the buckling wavelength increases and amplitude decreases, which behaves in a similar way as an accordion bellow. The big wave can be stretched up to the level of the pre-strain without cracking, such as 60% for Fig. 2(b). The stretchability of the hanging-over serpentine ZnO nanoribbons is through the twisting of the hanging-over segment, which is similar to stretching the coiled telephone cord. Figure 2(d) shows an optical image of a hanging-over serpentine ZnO nanoribbon subject to 30% stretching, where the twisting is observed.

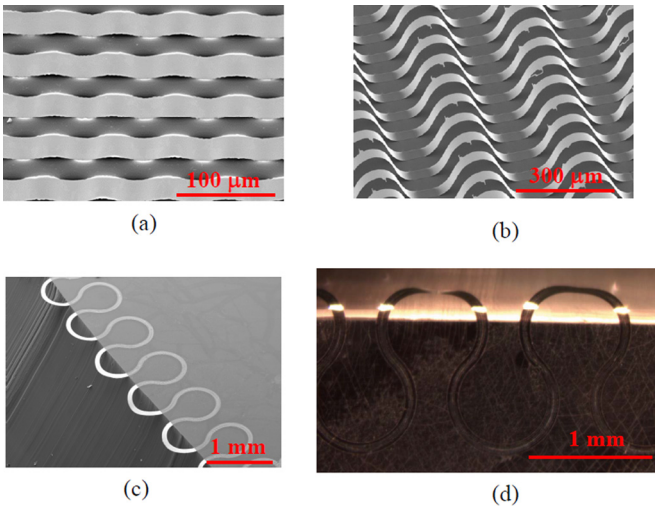

FIG. 2. Experimental images of pre-patterned ZnO nanoribbons on PDMS substrates. The thickness of ZnO nanoribbons is 370 nm. (a) A 47° tilted view of a SEM image of small waves. The pre-strain is 5% and the buckling wavelength is 60.2 μm. (b) A 47° tilted view of an SEM image of big waves with $W_{act} = 20\,\mu$m, $W_{in} = 480\,\mu$m, and $\varepsilon_{pre} = 60\%$. The buckling wavelength is 292 μm. (c) An SEM image of a hanging-over serpentine ZnO nanoribbon. (d) An optical micrograph showing a hanging-over serpentine subject to 30% applied strain, where the twisting at the overhanging segment is observed.

IV. DISCUSSION

The dynamic properties of these three configurations of pre-patterned ZnO nanoribbons are theoretically examined for energy harvesting applications. As the small waves are firmly bonded on PDMS, any mechanical vibrations on ZnO nanoribbons are damped by PDMS, which dissipates the vibration energy stored in ZnO nanoribbons rapidly. Thus, the small wave structure is not suitable for energy harvesting application though there are some efforts to utilize this structure as a platform to develop stretchable energy harvesting devices but no meaningful experimental measurements exist for harvested energy yet.

For big waves, the dynamic analysis[30] has found that the fundamental natural frequency $\Omega/\left(\sqrt{E_{ZnO}/(12\rho_{ZnO})}h_{ZnO}/W_{in}^2\right)$ does not depend on the level of strain and remains a constant (7.06) as long as $(\varepsilon_{pre}-\varepsilon_{applied})/[(1+\varepsilon_{pre})\varepsilon_{cr}] > 3.4$, where Ω is the fundamental natural frequency, $\rho = 5610\,\mathrm{kg/m^3}$ is the density of ZnO, $\varepsilon_{applied}$ is the applied strain on the buckled structure, $\varepsilon_{cr} = (\pi h_{\mathrm{Zno}}/W_{in})^2/3$ is the critical strain for pop-up buckling.[21] For nanoribbons (i.e., h_{ZnO}/W_{in} is on the order of 10^{-4}), ε_{pre} is much greater than ε_{cr} so that the criterion $(\varepsilon_{pre}-\varepsilon_{applied})/[(1+\varepsilon_{pre})\varepsilon_{cr}] > 3.4$ for strain-independent fundamental natural frequency holds as long as $\varepsilon_{applied}$ does not reach ε_{pre}. Though the analysis is for small deformation but the strain-independence of natural frequency to strain has been validated through finite element simulations, details seen in the supplementary material.[31] This relation is critical to develop stretchable energy harvesting devices, as upon deformation, the frequency range harvested by the structure does not prominently vary. The fundamental natural frequency is very important to energy harvesting and always designed to match the environmental frequency through the selection of geometric dimension of the structure. Due to the invariance of the fundamental natural frequency to pre-strain, the length and thickness of the ZnO nanoribbons can be designed through the equation $\Omega/\left(\sqrt{E_{ZnO}/(12\rho_{ZnO})}h_{ZnO}/W_{in}^2\right) = 7.06$ for given fundamental

natural frequency Ω, elastic modulus E, and density ρ of ZnO. Figure 3(a) provides a phase diagram of the natural frequency Ω as a function of h_{ZnO} and W_{in}. We are particularly interested in letting the natural frequency fall into the range of audio frequency (20 to 20 000 Hz), since the audio frequency exists everywhere in the ambient environment and provides a wide range to harness the vibration energy from the environment. The natural frequency of the big wave with $h_{ZnO} = 370$ nm and $W_{in} = 480\,\mu$m shown in Fig. 2(b) falls into range of audio frequency.

Another important factor in energy harvesting is that the external vibration sources have a wide spectrum of frequencies,[20] such as 20 to 20 000 Hz for audio frequency. The random analysis was conducted for big waves to determine the dynamic response under random excitation. The details were given in the supplementary material.[31] The external random vibration sources alter the buckling profiles and the associated bending energy, which can be converted to electrical energy. Thus, the expectation of the change of bending curvature under random excitation provides a means to find out the location of maximum harvestable bending energy, which is practically important for the energy harvesting devices. Figure 3(b) shows the distribution of normalized mean-square value of bending curvature change $E[v''^2]$ upon random excitation for different damping μ, along the ribbon direction. It is found that the maximal mean-square value of bending curvature change appears at $x/W_{in} = 0$ and 1, which corresponds to the anchor points between the activated and inactivated areas. Other extreme values appear at $x/W_{in} \approx 1/4$, 1/2, and 3/4 and the expectation at $x/W_{in} \approx 1/4$ and 3/4 is larger than that at $x/W_{in} \approx 1/2$. In energy harvest application, to reach large energy output, the electrodes should be placed at the locations with maximal mean-square value of bending curvature change, or equivalently, the maximal harvestable bending energy. Figure 3(b) actually suggests the optimal locations of the electrode at $x/W_{in} = 0$ and 1 and then $x/W_{in} \approx 1/4$ and 3/4.

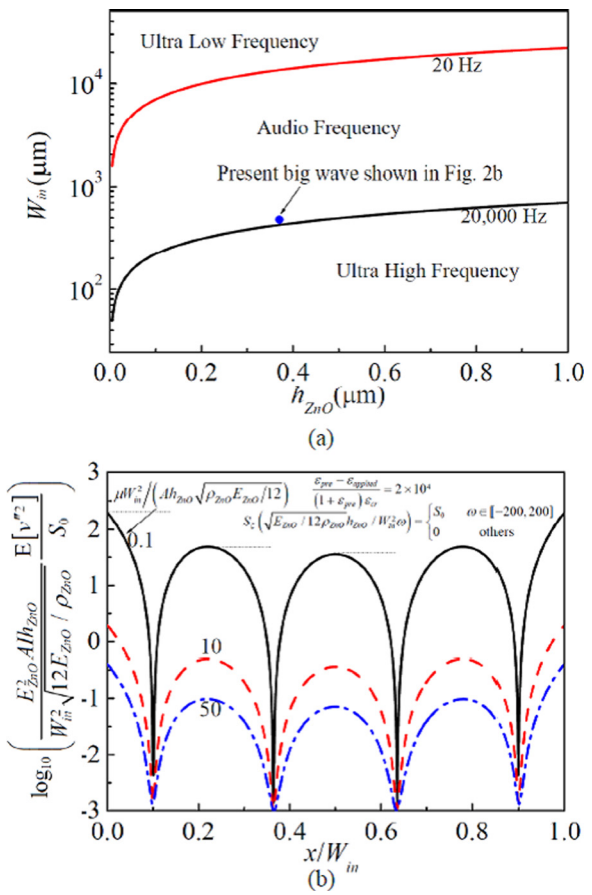

FIG. 3. Theoretical analysis of the dynamic behavior of big waves. (a) Phase diagram of the fundamental natural frequency of big waves by choosing the thickness of the nanoribbons (h_{ZnO}) and the patterning of the PDMS substrates (W_{in}). Three distinct frequency domains are shown, namely ultra-low frequency, audio frequency, and ultra-high frequency. The big waves in Fig. 2(b) fall into the audio frequency domain. A is the cross-sectional area and I is the moment of inertia. (b) The mean-square value of bending curvature change $E[v''^2]$ upon random excitations, normalized by the strength of the power spectrum density S_0 of the random excitation, as a function of normalized location x/W_{in} for different damping factor μ. Here, the power density spectrum $S_\xi(\omega)$ of the random excitation is taken as constant S_0 at $\omega \in [-200, 200]$ and 0 otherwise; the strain is taken as $(\varepsilon_{pre} - \varepsilon_{applied})/[(1+\varepsilon_{pre})\varepsilon_{cr}] = 2 \times 10^4$, where $\varepsilon_{applied}$ is the applied strain on the big waves and $\varepsilon_{cr} = (\pi h_{Zno}/W_{in})^2/3$ is the critical strain for big waves.

For serpentine structures without displacement loading, the fundamental natural frequency was estimated by using the beam theory and given by $\Omega = 0.56 h_{ZnO} \sqrt{E_{ZnO}/12\rho_{ZnO}}/l_{eff}^2$, where l_{eff} is the equivalent length of the serpentine structure and is selected as the length of the cantilever part. For the structure shown in Fig. 2(c), the length of the cantilever part, or the equivalent length $l_{eff} = 345\,\mu$m, the natural frequency is approximately 2407.7 Hz, which is in the audio frequency range. This indicates that the serpentine structure is capable to harvest the vibration energy in the ambient environment, which is in audio frequency range. The finite element simulations were also conducted to study the relationship between frequency and applied strain, as shown in the supplementary material.[31] Figure 4 shows the fundamental frequency as a function of applied strain. It is found that at vanishing applied strain, the fundamental natural frequency is 1472.8 Hz, on the same order of that obtained from the approximated beam theory. As strain increases, the natural frequency varies steadily but remains at the audio frequency range even at the 15%

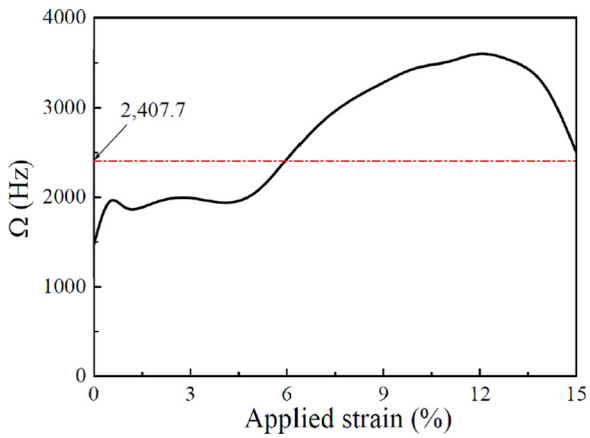

FIG. 4. Theoretical analysis of the dynamic behavior of hanging-over serpentine ZnO nanoribbons. Finite element simulation results are shown as the plot of fundamental natural frequency Ω as a function of applied strain. It is found that the fundamental natural frequency remains in the audio frequency domain and does not strongly depend on applied strain.

applied strain. With increase of the length of the cantilever part, the frequency has less dependence on the applied strain. Again interestingly, the over-hanging serpentine structure provides another design of reaching audio and strain insensitive frequency for harvesting ambient energy in audio frequency range.

V. CONCLUSIONS

Three forms of ZnO nanoribbons on PDMS substrates were fabricated through lithography patterning, namely small waves, big waves, and overhanging serpentine structures, and their applications on stretchable energy harvesting were discussed through theoretical analysis. It was found that big wave and overhanging serpentine structures show strain-insensitive fundamental natural frequencies in the audio frequency range upon applied strain, which provides a means to develop stretchable energy harvesting devices for various applications. Though the demonstration in this paper is for ZnO, the methodology can be applied to other piezoelectric materials, such as PZT with much stronger electrical-mechanical coupling. We expect that this work is able to enlighten a broad field of stretchable energy harvesting devices within audio frequency range. We also notice that the analysis in this paper does not consider multilayer structures that are employed in the real devices, though the similar analysis can be conducted by using the effective material properties of the multilayer structures.

ACKNOWLEDGMENTS

T.M. acknowledges the financial support from the China Scholarship Council. Y.W. acknowledges the National Natural Science Foundation of China under Grant No. 11002077. H.J. acknowledges the support from NSF CMMI-0700440. H.J. and H.Y. acknowledge the support from NSF CMMI-0928502.

[1]Y. Qi, N. T. Jafferis, K. Lyons, C. M. Lee, H. Ahmad, and M. C. McAlpine, Nano Lett. **10**(2), 524–528 (2010).
[2]X. Feng, B. D. Yang, Y. M. Liu, Y. Wang, C. Dagdeviren, Z. J. Liu, A. Carlson, J. Y. Li, Y. G. Huang, and J. A. Rogers, ACS Nano **5**(4), 3326–3332 (2011).
[3]Y. Qi, J. Kim, T. D. Nguyen, B. Lisko, P. K. Purohit, and M. C. McAlpine, Nano Lett. **11**(3), 1331–1336 (2011).
[4]T. D. Nguyen, N. Deshmukh, J. M. Nagarah, T. Kramer, P. K. Purohit, M. J. Berry, and M. C. McAlpine, Nat. Nanotechnol. **7**(9), 587–593 (2012).
[5]K. I. Park, S. Xu, Y. Liu, G. T. Hwang, S. J. L. Kang, Z. L. Wang, and K. J. Lee, Nano Lett. **10**(12), 4939–4943 (2010).
[6]K. I. Park, S. Y. Lee, S. Kim, J. Chang, S. J. L. Kang, and K. J. Lee, Electrochem. Solid-State Lett. **13**(7), G57–G59 (2010).
[7]H. C. Seo, I. Petrov, H. Jeong, P. Chapman, and K. Kim, Appl. Phys. Lett. **94**(9), 092104 (2009).
[8]Z. L. Wang and J. H. Song, Science **312**(5771), 242–246 (2006).
[9]R. Yang, Y. Qin, C. Li, G. Zhu, and Z. L. Wang, Nano Lett. **9**(3), 1201–1205 (2009).
[10]R. S. Yang, Y. Qin, L. M. Dai, and Z. L. Wang, Nat. Nanotechnol. **4**(1), 34–39 (2009).
[11]S. Xu, Y. Qin, C. Xu, Y. G. Wei, R. S. Yang, and Z. L. Wang, Nat. Nanotechnol. **5**(5), 366–373 (2010).
[12]L. Baeten, B. Conings, H. G. Boyen, J. D'Haen, A. Hardy, M. D'Olieslaeger, J. V. Manca, and M. K. Van Bael, Adv. Mater. **23**(25), 2802–2805 (2011).
[13]Y. Li, P. Lu, M. Jiang, R. Dhakal, P. Thapaliya, Z. Peng, B. Jha, and X. Yan, J. Phys. Chem. C **116**(48), 25248–25256 (2012).
[14]X. D. Bai, P. X. Gao, Z. L. Wang, and E. G. Wang, Appl. Phys. Lett. **82**(26), 4806–4808 (2003).
[15]J. Casals-Terre, A. Fargas-Marques, and A. M. Shkel, J. Microelectromech. Syst. **17**(5), 1082–1093 (2008).
[16]F. Cottone, H. Vocca, and L. Gammaitoni, Phys. Rev. Lett. **102**(8), 080601 (2009).
[17]A. F. Arrieta, P. Hagedorn, A. Erturk, and D. J. Inman, Appl. Phys. Lett. **97**(10), 104102 (2010).
[18]S. M. Jung and K. S. Yun, Appl. Phys. Lett. **96**(11), 111906 (2010).
[19]N. A. Khovanova and I. A. Khovanov, Appl. Phys. Lett. **99**(14), 144101 (2011).
[20]F. Cottone, L. Gammaitoni, H. Vocca, M. Ferrari, and V. Ferrari, Smart Mater. Struct. **21**(3), 035021 (2012).
[21]Y. Wang, T. Ma, H. Yu, and H. Jiang, Appl. Phys. Lett. **102**(4), 041915 (2013).
[22]D. C. Duffy, J. C. McDonald, O. J. A. Schueller, and G. M. Whitesides, Anal. Chem. **70**(23), 4974–4984 (1998).
[23]M. Ouyang, C. Yuan, R. J. Muisener, A. Boulares, and J. T. Koberstein, Chem. Mater. **12**(6), 1591–1596 (2000).
[24]W. R. Childs, M. J. Motala, K. J. Lee, and R. G. Nuzzo, Langmuir **21**(22), 10096–10105 (2005).
[25]Y. G. Sun, W. M. Choi, H. Q. Jiang, Y. G. Y. Huang, and J. A. Rogers, Nat. Nanotechnol. **1**(3), 201–207 (2006).
[26]D. Y. Khang, H. Q. Jiang, Y. Huang, and J. A. Rogers, Science **311**(5758), 208–212 (2006).
[27]A. Bietsch and B. Michel, J. Appl. Phys. **88**(7), 4310–4318 (2000).
[28]G. Mantini, Y. F. Gao, A. D'Amico, C. Falconi, and Z. L. Wang, Nano Res. **2**(8), 624–629 (2009).
[29]H. Jiang, Y. Sun, J. A. Rogers, and Y. Y. Huang, Appl. Phys. Lett. **90**, 133119 (2007).
[30]Y. Wang and X. Feng, Appl. Phys. Lett. **95**(23), 231915 (2009).
[31]See supplementary material at http://dx.doi.org/10.1063/1.4807320 for finite element analysis of big waves in large deformation and mode shapes of big waves, random analysis of big waves, and finite element analysis of hanging-over serpentine structure.

Supplemental Material
Pre-patterned ZnO Nanoribbons on Soft Substrates for Stretchable Energy Harvesting Applications

Teng Ma[1], Yong Wang[1,2], Rui Tang[3], Hongyu Yu[3], and Hanqing Jiang[1,a)]

[1]*School for Engineering of Matter, Transport and Energy, Arizona State University, Tempe, AZ 85287, USA*

[2]*Department of Engineering Mechanics, Zhejiang University, Hangzhou, Zhejiang 310027, China*

[3]*School of Electrical, Computer and Energy Engineering, Arizona State University, Tempe, AZ 85287, USA*

Finite Element Analysis of Big Waves in Large Deformation

Mode Shapes of Big Waves

Random Analysis of Big Waves

Finite Element Analysis of Hanging-Over Serpentine Structures

[a)] Email: hanqing.jiang@asu.edu

Finite Element Analysis of Big Waves in Large Deformation

To verify the theoretical analysis about the invariance of the fundamental natural frequency of big waves to applied displacement, the commercial finite element package ABAQUS was used to analyze the postbuckling behavior and the fundamental natural frequency vibrating around the postbuckling configuration. One element of big waves is modeled by 100 beam elements (B21) in ABAQUS. In order to investigate the postbuckling behavior of big waves, the buckling analysis subject to applied displacement is first implemented to obtain the eigen modes and then the imperfection with maximal value $10h_{ZnO}$ is introduced in big waves based on the eigen modes. Implementing the static analysis for big waves with initial imperfection yields the postbuckling configuration, and then the fundamental natural frequency of big waves vibrating around the postbuckling configuration is obtained. The first-order modal shape around the postbuckling configuration is shown in Fig. S1 for $\left(\varepsilon_{pre}-\varepsilon_{applied}\right)\big/\left(1+\varepsilon_{pre}\right)=0.4$. The fundamental natural frequency obtained through the ABAQUS simulation varies from 43,545 Hz to 33,901 Hz when $\left(\varepsilon_{pre}-\varepsilon_{applied}\right)\big/\left(1+\varepsilon_{pre}\right)$ varies from 1% to 50%, for geometric parameters $h_{ZnO}=370nm$ and $W_{in}=300\mu m$. Therefore, the fundamental natural frequency varies slowly when the structure is compressed or stretched remarkably, as shown in Fig. S2.

Mode Shapes of Big Waves

One element of the big wave can be modeled as a two-sidesclamped beam. Taking into account the geometric nonlinearity arising from mid-plane stretching,[1,2] the deflection *w* is prescribed by the following governing equation

$$\rho_{ZnO}A\frac{\partial^2 w}{\partial t^2}+E_{ZnO}I\frac{\partial^4 w}{\partial x^4}+\left[E_{ZnO}A\frac{\varepsilon_{pre}-\varepsilon_{applied}}{1+\varepsilon_{pre}}-\frac{E_{ZnO}A}{2W_{in}}\int_0^{W_{in}}\left(\frac{\partial w}{\partial x}\right)^2 \mathrm{d}x\right]\frac{\partial^2 w}{\partial x^2}=\xi \quad \text{(S1)}$$

where $A = bh_{ZnO}$ is the cross-sectional area with the width of b and $I = 1/(12bh_{ZnO}^3)$ is the moment of the inertia of the cross-section, μ and ξ are the damping factor and the uniformly distributed excitation, respectively. The boundary conditions are

$$w = 0, \frac{\partial w}{\partial x} = 0 \text{ at } x = 0, W_{in}. \tag{S2}$$

The static analysis gives the postbuckling configuration with respect to the applied strain,

$$w(x) = 2\sqrt{\frac{\varepsilon_{pre} - \varepsilon_{applied}}{\left(1+\varepsilon_{pre}\right)\varepsilon_{cr}} - 1}\left[1 - \cos\left(2\pi \frac{x}{W_{in}}\right)\right]. \tag{S3}$$

Remove the damping and excitation terms in Eq. (S1), the governing equation and the corresponding boundary conditions with respect to the small disturbance around the postbuckling configuration $v(x,t) = w(x,t) - w(x)$ are expressed as

$$\begin{aligned} &\rho_{ZnO} A \frac{\partial^2 v}{\partial t^2} + E_{ZnO} I \frac{\partial^4 v}{\partial x^4} + \frac{4\pi^2 E_{ZnO} I}{W_{in}^2} \frac{\partial^2 v}{\partial x^2} \\ &= \frac{E_{ZnO} A}{2W_{in}}\left[\frac{\partial^2 v}{\partial x^2}\int_0^{W_{in}}\left(\frac{\partial v}{\partial x}\right)^2 \mathrm{d}x + 2\frac{\partial^2 v}{\partial x^2}\int_0^{W_{in}} \frac{\partial v}{\partial x}\frac{\partial w}{\partial x}\mathrm{d}x + \frac{\partial^2 w}{\partial x^2}\int_0^{W_{in}}\left(\frac{\partial v}{\partial x}\right)^2 \mathrm{d}x + 2\frac{\partial^2 w}{\partial x^2}\int_0^{W_{in}} \frac{\partial v}{\partial x}\frac{\partial w}{\partial x}\mathrm{d}x\right] \end{aligned} \tag{S4}$$

$$v = 0, \frac{\partial v}{\partial x} = 0 \text{ at } x = 0, W_{in}. \tag{S5}$$

Neglecting the high-order terms and using the method of separation of variables, i.e., $v(x,t) = V(x)T(t)$, the solution of the space function $V(x)$ can be expressed as

$$V(x) = d_1 \sin(s_1 x) + d_2 \cos(s_1 x) + d_3 \sinh(s_2 x) + d_4 \cosh(s_2 x) + d_5 \frac{\partial^2 w}{\partial x^2} \tag{S6}$$

where $s_{1,2} = \sqrt{\pm 2\pi^2 + \sqrt{4\pi^4 + \omega^2}} \,/\, W_{in}$, $\omega = \Omega \Big/ \left(\sqrt{E_{ZnO}/(12\rho_{ZnO})}\, h_{ZnO}/W_{in}^2\right)$ is the non-dimensional natural frequency, in which Ω is the circular frequency, and d_5 satisfies the formula $\left\{\omega^2 - 32\pi^4\left[\frac{\varepsilon_{pre} - \varepsilon_{applied}}{\left(1+\varepsilon_{pre}\right)\varepsilon_{cr}} - 1\right]\right\} d_5 + \frac{12W_{in}^3}{h_{ZnO}^2}\int_0^{W_{in}} \frac{\partial}{\partial x}\left(V - d_5 \frac{\partial^2 w}{\partial x^2}\right)\frac{\partial w}{\partial x}\mathrm{d}x = 0$.

Substituting into the boundary conditions (S5) and solving the eigenvalue problem yield the non-dimensional natural frequencies $\omega_i \left(i = 1, 2, \cdots\right)$ and the corresponding mode shapes around the postbuckling configuration.

The first four-order modal shapes of big wave are given in Figure S3 for $(\varepsilon_{pre} - \varepsilon_{applied}) / [\left(1 + \varepsilon_{pre}\right) \varepsilon_{cr}] = 2.0 \times 10^4$. The first-order modal shape is the swing around the postbuckling configuration and there exists one node. This phenomenon apparently distinguishes from that of the planar beam, and the first-order modal shape of the latter is symmetric with respect to the mid-point and there does not exista node. The first-order and third-order modal shapes are asymmetric while the second-order and fourth-order modal shapes are symmetric.

Random Analysis of Big Waves

Suppose the random excitation $\xi(t)$ is bound-limited white noise with correlation function $R_\xi(\tau)$ and power spectrum density $S_\xi(\omega)$.[3] Substituting modal expansion $v(x,t) = \sum_i V_i(x) T_i(t)$ [4] into the governing equation, and then multiplying modal shapes $V_j(x)$ and integrating along the length of big waves yield the differential equation and frequency response function $H_i(\omega)$ with respect to $T_i(t)$.

The power spectrum density matrix of $T_i(t)$ then is expressed as,

$$\mathbf{S_T}(\omega) = \bar{\mathbf{H}}(\omega) \mathbf{H}^T(\omega) S_\xi(\omega) \tag{S7}$$

in which, "*bar*" and "*T*" denotes the conjugate and transpose, respectively.The curvature change induced by the disturbance, i.e., the curvature relative to the buckled configuration is $v''(x,t) = \sum_i V_i''(x) T_i(t)$, and so the mean-square value of the curvature change $v''(x_1,t)$ are expressed as,

$$E\left[v''^2\right]=\int_{-\infty}^{\infty}\mathbf{V}''^T(x)\cdot\bar{\mathbf{H}}(\omega)\cdot\mathbf{H}^T(\omega)\cdot\mathbf{V}''(x)S_{\xi}(\omega)\mathrm{d}\omega \tag{S8}$$

The detailed analysis is given elsewhere.[5]

Finite Element Analysis of Serpentine Structures

The commercial finite element package ABAQUS was used to analyze the postbuckling behavior of the hanging-over serpentine structure subject to applied strain and the dynamic property around the postbuckling configuration. The edge of the hanging-over serpentine structure is adhered to PDMS, and the other part is hanging over, as shown in Figure S4. The length of the cantilever part is about $345\mu m$. Due to the large thickness of the PDMS substrate compared to that of the ZnO film, the contact domain is modeled as fixed constrains. Hanging-over serpentine ZnO is modeled by 345 shell elements (S4 element) in ABAQUS.

In order to investigate the postbuckling configuration of the serpentine structure upon applied strain, the buckling analysis subject to applied displacement is first implemented to obtain the eigen modes and then the imperfection with maximal value $10h_{ZnO}$ is introduced in the serpentine structure based on the eigen modes. Implementing the static analysis for the hanging-over serpentine structure with initial imperfection yields the postbuckling configuration, and then the resonant frequency of the hanging-over serpentine structure vibrating around the postbuckling configuration is obtained. The postbuckling configuration and the first-order modal shape around the postbuckling configuration are shown in Figs. S5 and S6, respectively, for applied strain of 15%.

SM References

[1]A. H. Nayfeh, P. F. Pai, *Linear and Nonlinear Structural Mechanics*(Wiley-Interscience, New York, 2004).

[2]A. H. Nayfeh, S. A. Emam, Nonlinear Dyn.**54**, 395 (2008).

[3]E. Wong, B. Hajek, *Stochastic Processes in Engineering Systems* (Springer-Verlag, New York, 1985).

[4]Y. K. Lin, *Probabilistic Theory of Structural Dynamics* (McGRAW-HILL BOOK COMPANY, New York, 1967).

[5]Y. Wang, T. Ma, H. Yu, and H. Jiang, Appl. Phys. Lett.**102**, 041915 (2013).

SM Figure Captions

FIG. S1. Finite element results of the first-order modal shape of big waves vibrating around the postbuckling configuration.

FIG. S2. Finite element results of the invariance of fundamental natural frequency to the applied displacement.

FIG. S3. Analytical results of the first four-order modal shapes of big waves.

FIG. S4. Scanning electron micrograph showing the top view of the hanging-over serpentine structure.

FIG. S5. Finite element results of the postbuckling configuration of the hanging-over serpentine structure subject to applied strain 15% .

FIG. S6. Finite element results of the first-order modal shape of the hanging-over serpentine structure around the postbuckling configuration subject to applied strain 15% .

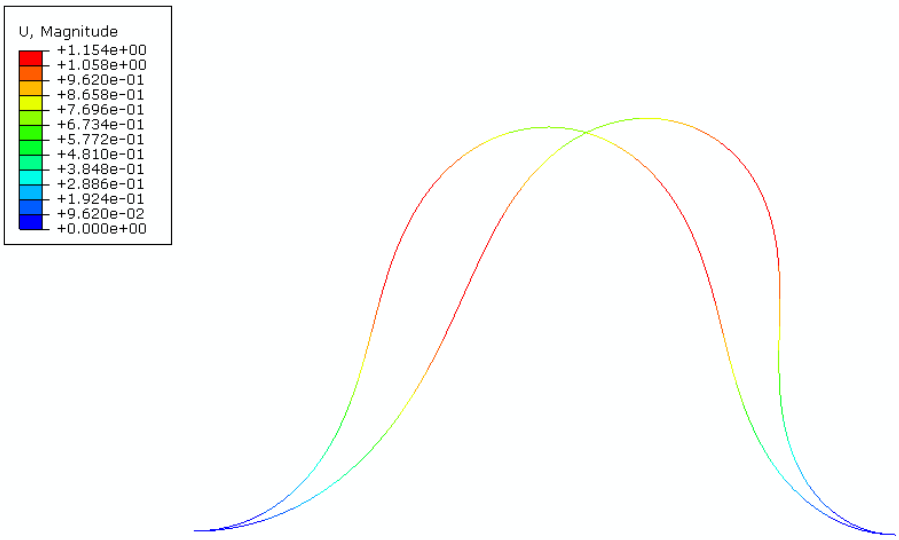
U, Magnitude
+1.154e+00
+1.058e+00
+9.620e-01
+8.658e-01
+7.696e-01
+6.734e-01
+5.772e-01
+4.810e-01
+3.848e-01
+2.886e-01
+1.924e-01
+9.620e-02
+0.000e+00

FIG. S1

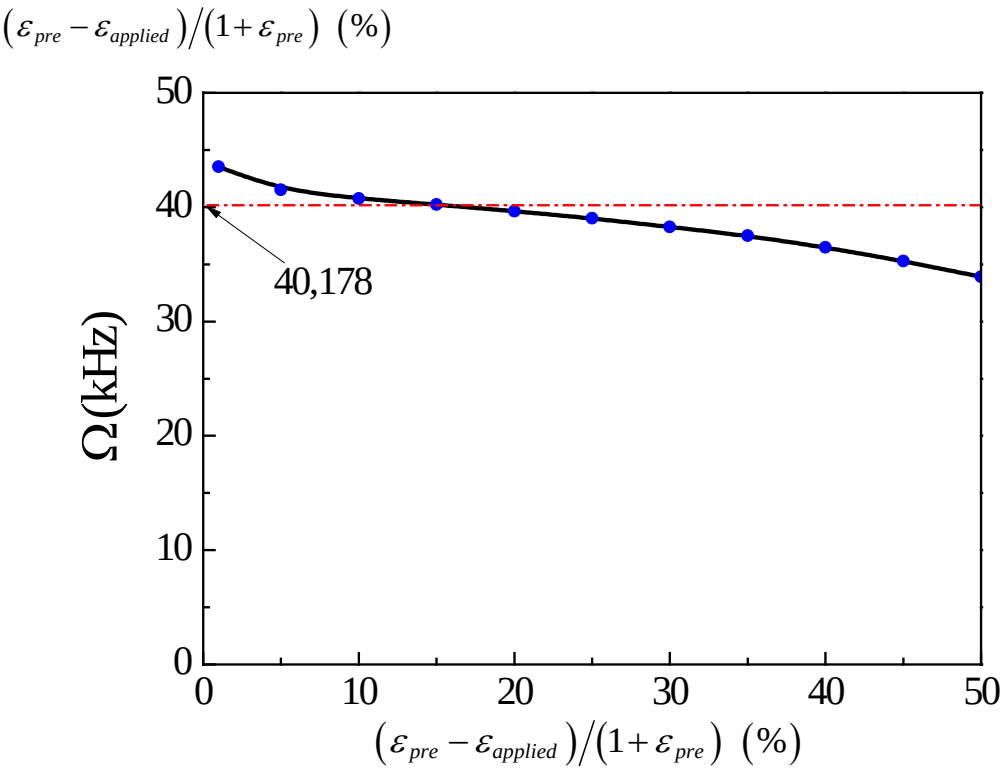
$(\varepsilon_{pre}-\varepsilon_{applied})/(1+\varepsilon_{pre})$ (%)
50
40
30
20
10
0
40,178
Ω(kHz)
0
10
20
30
40
50
$(\varepsilon_{pre}-\varepsilon_{applied})/(1+\varepsilon_{pre})$ (%)

FIG. S2

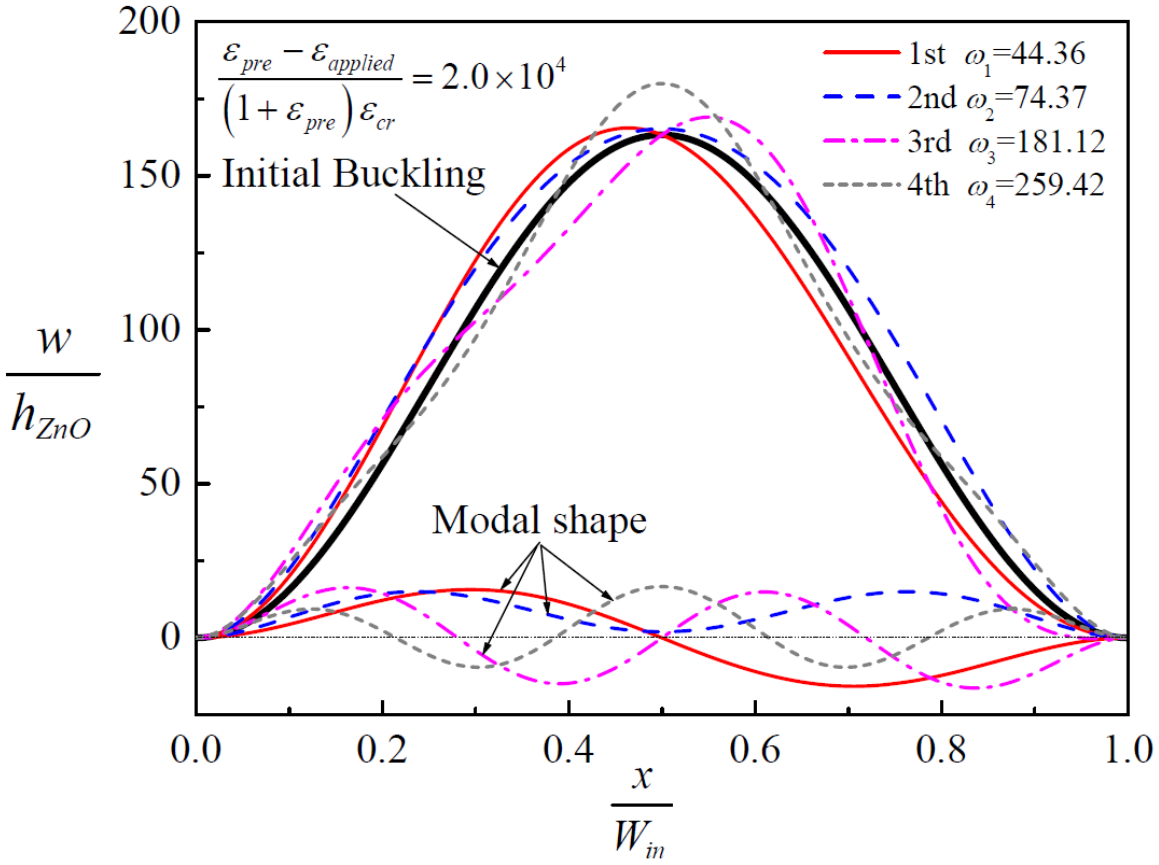
200
150
100
50
0
0.0
0.2
0.4
0.6
0.8
1.0
$\frac{w}{h_{ZnO}}$
$\frac{x}{W_{in}}$
$\frac{\varepsilon_{pre}-\varepsilon_{applied}}{(1+\varepsilon_{pre})\varepsilon_{cr}}=2.0\times10^{4}$
Initial Buckling
Modal shape
1st ω_1=44.36
2nd ω_2=74.37
3rd ω_3=181.12
4th ω_4=259.42

FIG. S3

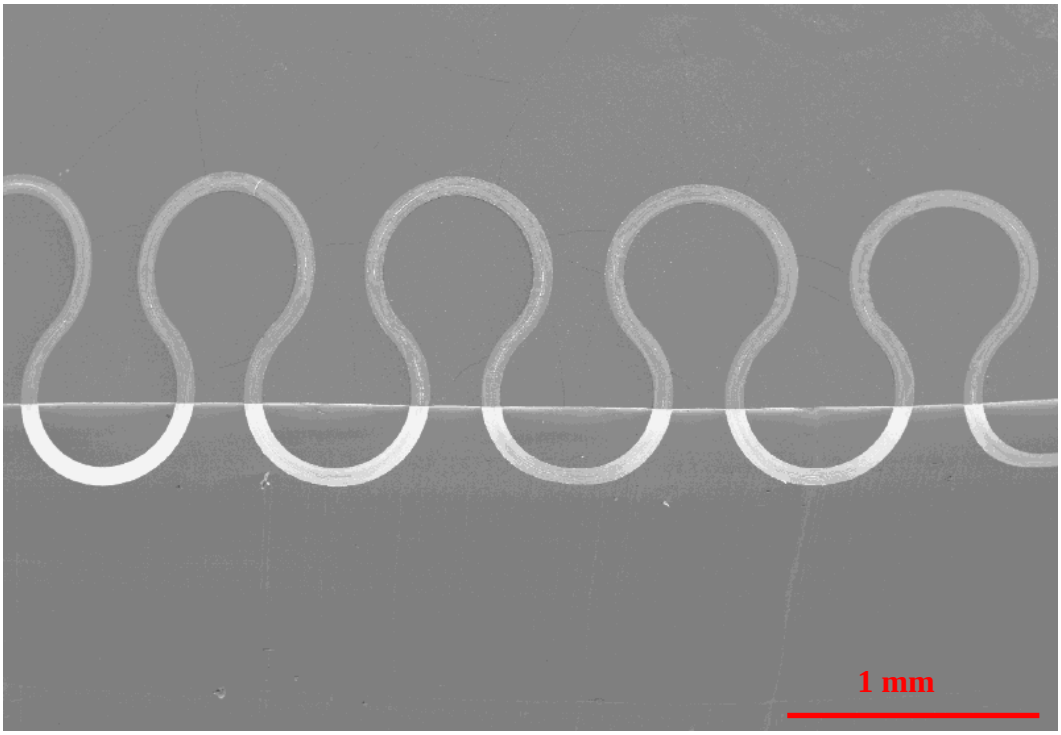

FIG. S4

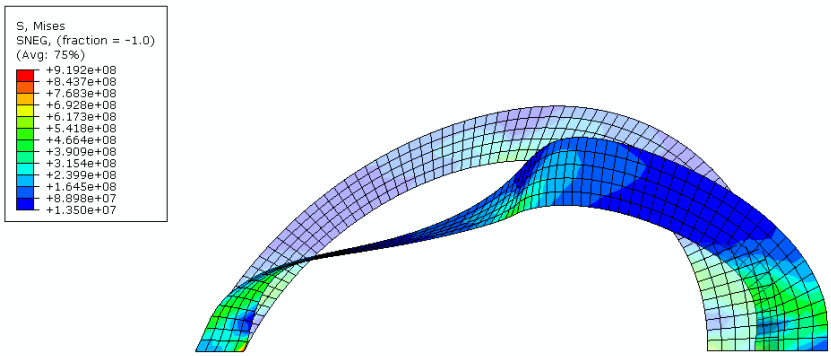
S, Mises
SNEG, (fraction = -1.0)
(Avg: 75%)
+9.192e+08
+8.437e+08
+7.683e+08
+6.928e+08
+6.173e+08
+5.418e+08
+4.664e+08
+3.909e+08
+3.154e+08
+2.399e+08
+1.645e+08
+8.898e+07
+1.350e+07

FIG. S5

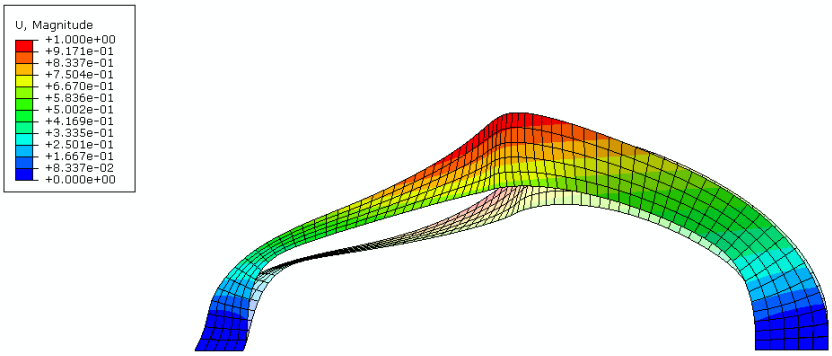
U, Magnitude
+1.000e+00
+9.171e-01
+8.337e-01
+7.504e-01
+6.670e-01
+5.836e-01
+5.002e-01
+4.169e-01
+3.335e-01
+2.501e-01
+1.667e-01
+8.337e-02
+0.000e+00

Figure S6